6

Inverse Position Procedure for Manipulators with Rotary Joints

Ibrahim A. Sultan

1. Introduction

Industrial robot manipulators are essentially spatial linkages that consist of rigid bodies connected by joints. Even though many types of joints (which are also known as kinematic pairs) are available for use in mechanical linkages, only two types are employed for robot manipulators. These are the revolute, or rotary, joints (referred to in literature as R) and the prismatic, or sliding, joints (referred to as P). These specific types allow a single degree of freedom relative movement between adjacent bodies; and are easier to drive and control than other kinematic pairs. Normally every joint on the manipulator is independently driven by a dedicated motor. It is central to kinematic control of manipulators to calculate the sets of joint-motor displacements which correspond to a desired pose (i.e. position and orientation) at the end-effector. The mathematical procedure which is followed to achieve this purpose is often referred to as, *Inverse Position Analysis*. This analysis presents a special difficulty in the field of Robotics as it is associated with the use of intricate spatial geometry techniques. The complexity of the analysis increases substantially with the number of rotary joints on the manipulator structure. For this reason a considerable part of the published literature is mainly concerned with the revolute-joint manipulators.

Published literature reveals that various methods have been proposed to solve the inverse position problem of manipulators. These methods range from Jacobian-based iterative techniques to highly sophisticated levels of equation-manipulation intended to reduce the whole model into a polynomial with thousands of mathematical terms. However, most industrial robots are designed with geometric features (such as parallelism and perpendicularity) to make it possible for simple inverse position solutions to be obtained in closed forms suitable for real time control. Another geometric aspect that leads to simplified inverse solutions is the spherical wrist design, which entails that the last three joints on the manipulator structure intersect at one point. This usually suggests that these three joints (also known as the wrist joints) have the main task of orienting (rather than placing) the end-effector in space. In this

case it should be possible to regard the manipulator as consisting of two separate parts where the first part (referred to as the arm) consists of the first three joints, counting from the stationary base, on the structure. The task of the arm is to place the end-effector origin (i.e. the point of intersection of the last three joint axes) at a defined point in space. The solution for this first part can be obtained separately before proceeding to find the angles of the last three joints which will result in giving the end-effector its desired spatial orientation. The work presented in this paper adopts this strategy to propose a mathematical procedure, for the arm inverse solution, based on assigning local coordinates at every joint, and utilising the properties of rotation to relate these coordinates. A model manipulation technique is then employed to obtain the arm inverse solution in terms of one polynomial. A kinematic synthesis discussion is then presented for the arm structure in terms of local coordinates to reflect on the number of solutions expected from the polynomial. It will be shown that the concept of intersecting spatial circles offers a good ground to comprehend the kinematics of revolute-joint manipulators. Moreover, models are presented for the wrist structure to obtain a full inverse kinematic solution for the robot manipulator. A solved example is demonstrated to prove the validity of the method presented.

2. Literature Survey

Published literature reveals that the homogeneous transformation matrix which was developed as far back as 1955 has extensively been employed for the analysis of robot manipulators. The matrix involves the use of four parameters, usually referred to as the DH-parameters, intended to perform transformation between two spatial Cartesian coordinate systems (Denavit and Hartenberg, 1955). Recently, other kinematic models have been proposed by researchers to deal with the drawbacks of the DH presentation (Sultan and Wager, 1999). This is particularly important if the model is going to be implemented for robot calibration purposes. The theory of dual-number algebra was introduced into the field of kinematics back in the 1960's (Yang and Freudenstein, 1964); and it did appeal to researchers in the field of robot kinematics (Pennock and Yang, 1985; Gu and Luh, 1987; Pardeep *et al*, 1989). In addition to these approaches, which are based on matrices, vector methods were also employed in the field of kinematic analysis of robots (Duffy, 1980; Lee and Liang, 1988A and 1988B).

Many industrial robots possess parallel and intersecting joint-axes and their direct-position models can be inverted analytically such that closed-form solutions may be obtained for the joint-displacements (Gupta, 1984; Pennock and Yang, 1985; Pardeep *et al*, 1989; Wang and Bjorke, 1989).

Spherical-wrist manipulators have their last three joint-axes intersecting at a common point. For these manipulators the position of the end-effector in space is determined only by the displacements performed about the first three joint-axes. This concept is often referred to as the position-orientation decoupling; and has been utilised to produce a closed form solution, for the inverse position problem of simple structure robots, efficient enough to be implemented for computer control (Pieper and Roth, 1969). Inverse position techniques have been proposed to utilise the position-orientation decoupling of industrial robot of arbitrarily directed axes (Sultan, 2000; Sultan and Wager, 2001). As such these techniques do not rely on any particular spatial relations (e.g. parallelism or perpendicularity) between the successive joint-axes. In fact, approaches which utilise these particular geometric features to produce the model equations are likely to produce positioning errors when used for robot control since the actual structures always deviate from their intended ideal geometry.

Iterative techniques have been employed for the inverse position analysis of general robot manipulators. Many of these techniques involve the computation of a Jacobian matrix which has to be calculated and inverted at every iteration. The solution in this case may be obtained by a Newton-Raphson technique (Hayati and Reston, 1986) or a Kalman filter approach (Coelho and Nunes, 1986). However, the inversion of the system Jacobian may not be possible near singular configurations (where the motion performed about one joint-axis produces exactly the same effect, at the end-effector, as the motion performed about another axis, hence resulting in loss of one or more degrees of freedom). Therefore, a singularity avoidance approach has been reported where the technique of damped least-squares is used for the analysis (Chiaverini *et al*, 1994). However, this technique seems to be rather sluggish near singular points where extra computational procedure may have to be involved.

Optimisation techniques have also been employed to solve the inverse-position problem of manipulators whereby a six-element error vector was implemented for the analysis (Goldenberg *et al*, 1985). The vector combines the current spatial information (position and orientation) of the robot hand and compares it to the desired pose to produce error values. Published literature in the area of optimisation report a technique by which the robot is moved about one joint at a time to close an error gap (Mahalingam and Sharan, 1987; Wang and Chen, 1991; Poon and Lawrence, 1988). More recent research effort demonstrates valuable inputs form such areas as neural networks (Zhang *et al*, 2005) and fuzzy techniques (Her *et al*, 2002) to the field of robot inverse kinematics.

It has been shown that the kinematic behaviour of robots can be described in terms of a set of polynomials that can be solved iteratively (Manseur and Doty 1992a, 1992b and 1996). One such method features a set of eight polynomials

which were solved numerically to obtain different possible solutions to the inverse position problem; it could therefore be concluded that the maximum number of meaningful solutions to the inverse position problem of a general robotic structure is 16 (Tsai and Morgan 1985), rather than 32 as had previously been suggested (Duffy and Crane, 1980). However it has been pointed out that a manipulator with 16 different real inverse position solutions can seldom be found in real life (Manseur and Doty, 1989). In reality most manipulators are designed to possess up to 8 solutions of which only one or two can be physically attained.

It is possible to express the inverse position problem of robots in terms of a 16 degree polynomial in the tan-half-angle of a joint-displacement (Lee and Liang 1988a & 1988b; Raghavan and Roth 1989). However it has been argued that the coefficients of such a polynomial are likely to contain too many terms which may render such a tack impractical to use (Smith and Lipkin 1990). Also, these high order polynomials are obtained by evaluating the eliminants of hyper-intricate determinants which may be impossible to handle symbolically in the first place. This may have motivated some researchers (Manocha and Canny 1992; Kohli and Osvatic 1993) to reformulate the solutions in terms of eigenvalue models in order to simplify the analysis and avoid numerical complications. However, a numerical technique has been introduced to obtain the inverse solutions without having to expand the system characteristic determinant (Sultan, 2002).

The procedure introduced here for the inverse position analysis of robot manipulators is described in the rest of this paper.

3. Rotation of Vectors

The unit vector $\hat{\mathbf{z}}_i$ in Figure (1) represents an axis of rotation in a spatial mechanism. It is required to obtain the new *rotated* vector, $\mathbf{v}_{ir}$, which results from rotating the *original* vector $\mathbf{v}_{io}$ (where $\mathbf{v}_{io} \times \hat{\mathbf{z}}_i \neq \mathbf{0}$) by an angle $\theta_i \hat{\mathbf{z}}_i$ In order to do so, the Cartesian system $\hat{\mathbf{x}}_i \hat{\mathbf{y}}_i \hat{\mathbf{z}}_i$ may be introduced as follows,

$$\hat{\mathbf{x}}_i \circ \hat{\mathbf{z}}_i = 0 \qquad (1)$$

where $\|\hat{\mathbf{x}}_i\| = 1$.

Then

$$\hat{\mathbf{y}}_i = \hat{\mathbf{z}}_i \times \hat{\mathbf{x}}_i \qquad (2)$$

The original vector, $\mathbf{v}_{io}$, and the rotated vector $\mathbf{v}_{ir}$, can both be expressed with respect to the $\hat{\mathbf{x}}_i \hat{\mathbf{y}}_i \hat{\mathbf{z}}_i$-frame in terms of local coordinates, *n*, *m* and *l* as follows,

$$\left.\begin{aligned}\mathbf{v}_{io} &= n_{io}\hat{\mathbf{x}}_i + m_{io}\hat{\mathbf{y}}_i + l_{io}\hat{\mathbf{z}}_i \\ \mathbf{v}_{ir} &= n_{ir}\hat{\mathbf{x}}_i + m_{ir}\hat{\mathbf{y}}_i + l_{ir}\hat{\mathbf{z}}_i\end{aligned}\right\} \quad (3)$$

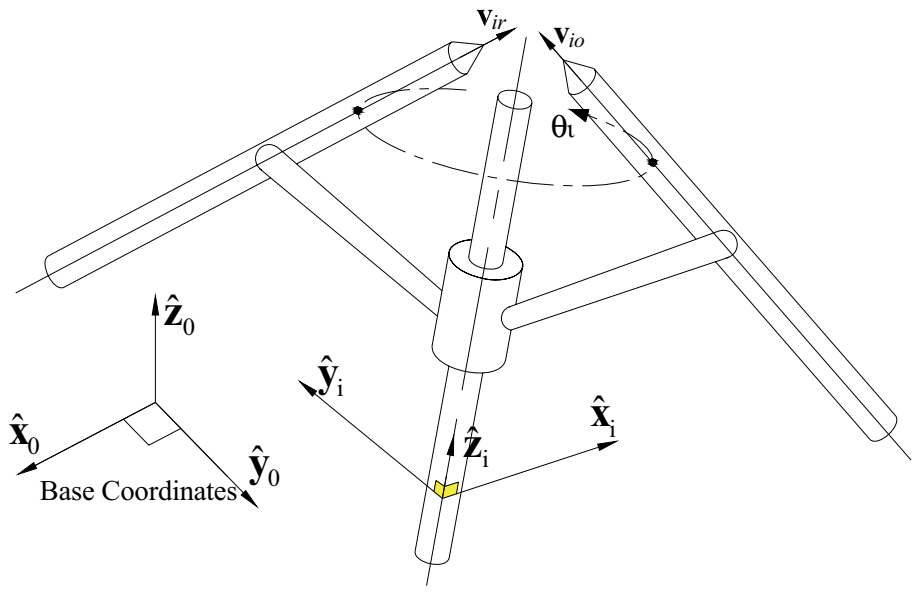

Figure 1. Rotation of Vectors.

where the local coordinates are given as follows;

$$\left.\begin{aligned}n_{io} &= \mathbf{v}_{io} \circ \hat{\mathbf{x}}_i \\ m_{io} &= \mathbf{v}_{io} \circ \hat{\mathbf{y}}_i \\ l_{io} &= \mathbf{v}_{io} \circ \hat{\mathbf{z}}_i\end{aligned}\right\} \quad (4)$$

And

$$\left.\begin{aligned}n_{ir} &= n_{io}\cos\theta_i - m_{io}\sin\theta_i \\ m_{ir} &= m_{io}\cos\theta_i + n_{io}\sin\theta_i \\ l_{ir} &= l_{io}\end{aligned}\right\} \quad (5)$$

The inverse of this problem is encountered when $\hat{\mathbf{z}}_i$, $\mathbf{v}_{io}$ and $\mathbf{v}_{ir}$ are all known and it is required to obtain the corresponding value of θ_i. With the values of the local coordinates known, θ_i could be obtained as follows,

$$\theta_i = \text{atan2}(m_{ir}n_{io} - n_{ir}m_{io}, n_{ir}n_{io} + m_{ir}m_{io}) \quad (6)$$

where the function atan2(y,x) is available in many computer algebra packages and compilers to compute the angle θ_i (over the range of the whole circle) when its sine and cosine are both given. In this paper, the concepts mentioned above are used together with the suitable conditions of rotation to perform the inverse position analysis of the manipulator arm and wrist. The proposed analysis for the arm is given in the next section.

4. Inverse Kinematics of the Arm

The arm, which is the largest kinematic part of the manipulator, consists of three revolute joints connected through rigid links. Each joint, as shown in Figure (2), is represented by the spatial pose of its axis. The first joint-axis has a fixed location and orientation in space as it represents the connection between the whole manipulator and the fixed frame. Any other joint-axis number *i* can float in space as it rotates about the joint-axis number *i*–1.

In the current context, the main function of the arm is to displace a certain spatial point from an initial known location to a required final position. In spherical-wrist manipulators, this point is at the intersection of the wrist axes. In a calibrated (non-spherical-wrist) manipulator, it may represent a point on the sixth axis as close as possible to the fifth joint-axis. In Figure (2), the arm is required to displace point pi to a final position pf. The position vectors, $\mathbf{pi}_b$ and $\mathbf{pf}_b$ respectively, of these two points are known with respect to the base coordinate system.

As per Appendix A, any joint-axis $\hat{\mathbf{z}}_i$ is related to the successive axis, $\hat{\mathbf{z}}_{i+1}$, through a common normal, $\hat{\mathbf{x}}_{i+1}$. This common normal is used to construct a local frame at the axis $\hat{\mathbf{z}}_{i+1}$ using the relation, $\hat{\mathbf{y}}_{i+1} = \hat{\mathbf{z}}_{i+1} \times \hat{\mathbf{x}}_{i+1}$. The shortest distance, a_{i+1}, between the axes, $\hat{\mathbf{z}}_i$ and $\hat{\mathbf{z}}_{i+1}$, is measured along $\hat{\mathbf{x}}_{i+1}$ which intersects $\hat{\mathbf{z}}_i$ at the point p_i and $\hat{\mathbf{z}}_{i+1}$ at the point $\mathrm{p}_{i(i+1)}$.

At the zero initial position which is shown in Figure (2), the axis $\hat{\mathbf{x}}_1$ is chosen to coincide with $\hat{\mathbf{x}}_2$. In this figure, the position vectors, $\mathbf{pi}_{3o}$ and $\mathbf{pf}_{1r}$, of points pi and pf respectively with respect to the frames $\hat{\mathbf{x}}_3\hat{\mathbf{y}}_3\hat{\mathbf{z}}_3$ and $\hat{\mathbf{x}}_1\hat{\mathbf{y}}_1\hat{\mathbf{z}}_1$ may be numerically calculated as follows,

$$\left.\begin{aligned} \mathbf{pf}_{1r} &= \mathbf{pf}_b - \mathbf{p}_1 \\ \mathbf{pi}_{3o} &= \mathbf{pi}_b - \mathbf{p}_{32} \end{aligned}\right\} \tag{7}$$

where $\mathbf{p}_1$ and $\mathbf{p}_{32}$ are the position vectors of the axes-attached, points p_1 and p_{32}, respectively as measured from the origin of the base coordinates. Accord-

ing to the concepts in (4) and (5), $\mathbf{pf}_{1r}$ can be described with respect to the $\hat{\mathbf{x}}_1\hat{\mathbf{y}}_1\hat{\mathbf{z}}_1$-frame in terms of known local coordinates (n_{1r}, m_{1r} and l_{1r}). Also, $\mathbf{pi}_{30}$ can be described with respect to the $\hat{\mathbf{x}}_3\hat{\mathbf{y}}_3\hat{\mathbf{z}}_3$-frame in terms of known local coordinates (n_{3o}, m_{3o} and l_{3o}).

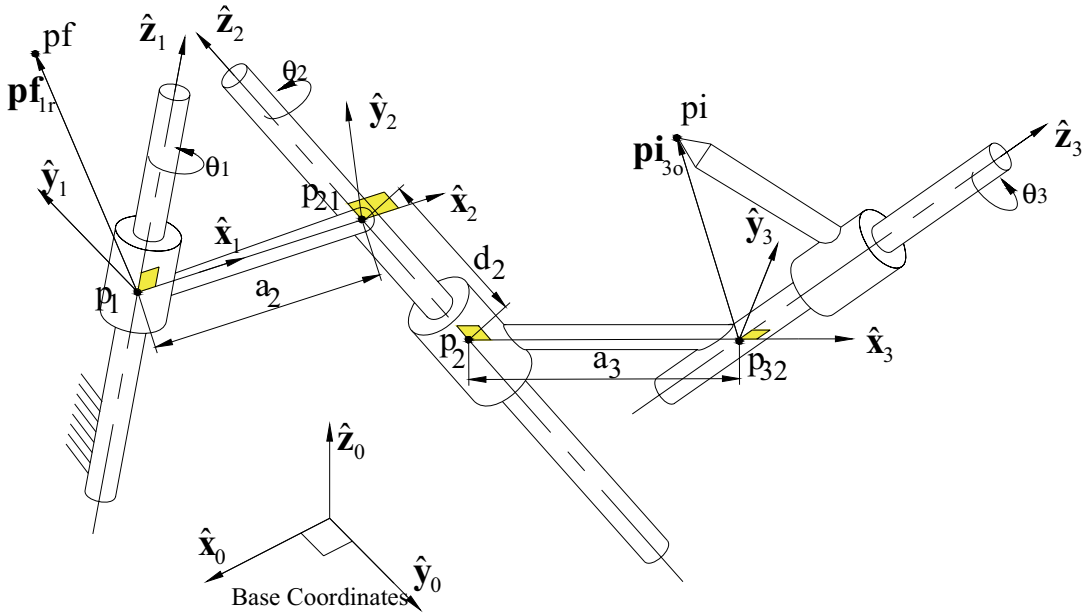

Figure 2. A General View of a 3R Manipulator Arm at Its Zero Position.

It is understood that the vector $\mathbf{pf}_{1r}$ resulted from rotating another vector $\mathbf{pf}_{1o}$ about the $\hat{\mathbf{z}}_i$ axis by an angle, θ_1 (i.e. a $\theta_1\hat{\mathbf{z}}_1$-type rotation). The original vector, $\mathbf{pf}_{1o}$, can be expressed with respect to the $\hat{\mathbf{x}}_1\hat{\mathbf{y}}_1\hat{\mathbf{z}}_1$-frame in terms of local coordinates (n_{1o}, m_{1o} and l_{1o}). Also, during the positioning process the vector $\mathbf{pi}_{3o}$ will perform a $\theta_3\hat{\mathbf{z}}_3$-type rotation to evolve into $\mathbf{pi}_{3r}$ which can be expressed with respect to the $\hat{\mathbf{x}}_3\hat{\mathbf{y}}_3\hat{\mathbf{z}}_3$-frame in terms of local coordinates (n_{3r}, m_{3r} and l_{3r}). Therefore the two vectors, $\mathbf{pf}_{1o}$ and $\mathbf{pi}_{3r}$ can be written as follows;

$$\left.\begin{aligned}\mathbf{pf}_{1o} &= n_{1o}\hat{\mathbf{x}}_1 + m_{1o}\hat{\mathbf{y}}_1 + l_{1o}\hat{\mathbf{z}}_1\\ \mathbf{pi}_{3r} &= n_{3r}\hat{\mathbf{x}}_3 + m_{3r}\hat{\mathbf{y}}_3 + l_{3r}\hat{\mathbf{z}}_3\end{aligned}\right\} \tag{8}$$

where the two equations above have four unknowns that need to be determined. These four unknowns are n_{1o}, m_{1o}, n_{3r} and m_{3r}. The numerical values of the *l*-type local coordinates are calculated as follows;

$$\left.\begin{aligned} l_{3r} &= \mathbf{pi}_{3o} \circ \hat{\mathbf{z}}_3 \\ l_{1o} &= \mathbf{pf}_{1r} \circ \hat{\mathbf{z}}_1 \end{aligned}\right\} \tag{9}$$

In fact the value of l_{3r} is calculated, and stored in a data file, once the manipulator has been calibrated and an initial position has been nominated; however, l_{1o} has to be calculated for every new desired end-effector position. Moreover, the end-effector positions which are defined by the vectors $\mathbf{pf}_{1o}$ and $\mathbf{pi}_{3r}$ can be used to study the rotation about the middle joint-axis, $\hat{\mathbf{z}}_2$. These same positions can be expressed relative to a point, p_2, attached to $\hat{\mathbf{z}}_2$, using the two respective vectors, $\mathbf{p}_{2r}$ and $\mathbf{p}_{20}$ as follows;

$$\left.\begin{aligned} \mathbf{p}_{2r} &= \mathbf{pf}_{1o} + d_2\hat{\mathbf{z}}_2 - a_2\hat{\mathbf{x}}_2 \\ \mathbf{p}_{2o} &= \mathbf{pi}_{3r} + a_3\hat{\mathbf{x}}_3 \end{aligned}\right\} \tag{10}$$

where $d_2 = (\mathbf{p}_{21} - \mathbf{p}_2) \circ \hat{\mathbf{z}}_2$

It may be noted that $\mathbf{p}_{2r}$ and $\mathbf{p}_{20}$ are separated by a single rotation, $\theta_2\hat{\mathbf{z}}_2$. The properties of this rotation may be utilised to show that,

$$\mathbf{pi}_{2o} \circ \hat{\mathbf{z}}_2 = \mathbf{pi}_{2r} \circ \hat{\mathbf{z}}_2 \tag{11}$$

and

$$\mathbf{pi}_{2o} \circ \mathbf{pi}_{2o} = \mathbf{pi}_{2r} \circ \mathbf{pi}_{2r} \tag{12}$$

Equations (7) to (12) may then be manipulated to obtain the following two linear equations,

$$m_{1o}\hat{\mathbf{y}}_1 \circ \hat{\mathbf{z}}_2 = m_{3r}\hat{\mathbf{y}}_3 \circ \hat{\mathbf{z}}_2 + l_{3r}\hat{\mathbf{z}}_3 \circ \hat{\mathbf{z}}_2 - l_{1o}\hat{\mathbf{z}}_1 \circ \hat{\mathbf{z}}_2 - d_2 \tag{13}$$

and

$$m_{1o}d_2\hat{\mathbf{y}}_1 \circ \hat{\mathbf{z}}_2 - a_2n_{1o} = a_3n_{3r} + \frac{1}{2}\left(\mathbf{pi}_{3i} \circ \mathbf{pi}_{3i} - \mathbf{pf}_{1r} \circ \mathbf{pf}_{1r} + a_3^2 - a_2^2 - d_2^2 - 2l_{1o}d_2\hat{\mathbf{z}}_1 \circ \hat{\mathbf{z}}_2\right) \tag{14}$$

The concept in equations (3) and (5) may be employed to express the x_2-, y_2- and z_2-components of a rotated vector $\mathbf{p}_{2o}^r$ which results from performing a $\theta_2\hat{\mathbf{z}}_2$ rotation on $\mathbf{p}_{20}$. Then the coincidence of $\mathbf{p}_{2o}^r$ and $\mathbf{p}_{2r}$ may be described by,

$$\mathbf{p}_{2o}^{r} \circ \hat{\mathbf{x}}_2 = \mathbf{p}_{2r} \circ \hat{\mathbf{x}}_2 \tag{15}$$

and

$$\mathbf{p}_{2o}^{r} \circ \hat{\mathbf{y}}_2 = \mathbf{p}_{2r} \circ \hat{\mathbf{y}}_2 \tag{16}$$

where $\mathbf{p}_{2o}^{r} \circ \hat{\mathbf{z}}_2 = \mathbf{p}_{2r} \circ \hat{\mathbf{z}}_2$ is already described in equation (13) , and the expanded forms of the (15) and (16) are given respectively as follows;

$$\begin{aligned} n_{1o} - a_2 = {} & \left(\hat{\mathbf{x}}_3 \circ \hat{\mathbf{x}}_2 c_2 - \hat{\mathbf{x}}_3 \circ \hat{\mathbf{y}}_2 s_2\right) n_{3r} + \left(\hat{\mathbf{y}}_3 \circ \hat{\mathbf{x}}_2 c_2 - \hat{\mathbf{y}}_3 \circ \hat{\mathbf{y}}_2 s_2\right) m_{3r} \\ & + \left(l_{3r} \hat{\mathbf{z}}_3 \circ \hat{\mathbf{x}}_2 + a_3 \hat{\mathbf{x}}_3 \circ \hat{\mathbf{x}}_2\right) c_2 - \left(l_{3r} \hat{\mathbf{z}}_3 \circ \hat{\mathbf{y}}_2 + a_3 \hat{\mathbf{x}}_3 \circ \hat{\mathbf{y}}_2\right) s_2 \end{aligned} \tag{17}$$

and

$$\begin{aligned} m_{1o} \hat{\mathbf{y}}_1 \circ \hat{\mathbf{y}}_2 + l_{1o} \hat{\mathbf{z}}_1 \circ \hat{\mathbf{y}}_2 = {} & \left(\hat{\mathbf{x}}_3 \circ \hat{\mathbf{x}}_2 s_2 + \hat{\mathbf{x}}_3 \circ \hat{\mathbf{y}}_2 c_2\right) n_{3r} + \left(\hat{\mathbf{y}}_3 \circ \hat{\mathbf{x}}_2 s_2 + \hat{\mathbf{y}}_3 \circ \hat{\mathbf{y}}_2 c_2\right) m_{3r} \\ & + \left(l_{3r} \hat{\mathbf{z}}_3 \circ \hat{\mathbf{y}}_2 + a_3 \hat{\mathbf{x}}_3 \circ \hat{\mathbf{y}}_2\right) c_2 + \left(l_{3r} \hat{\mathbf{z}}_3 \circ \hat{\mathbf{x}}_2 + a_3 \hat{\mathbf{x}}_3 \circ \hat{\mathbf{x}}_2\right) s_2 \end{aligned} \tag{18}$$

where c_2 and s_2 stand for $\cos\theta_2$ and $\sin\theta_2$ respectively.

The four linear equations, (13), (14), (17) and (18) represent the mathematical core of the kinematic model introduced in the present work for the inverse position analysis of the arm module. A symbolic solution for these equations can be obtained such that, n_{3r} and m_{3r} are expressed in the following forms,

$$n_{3r} = f_1 / f \tag{19}$$

and

$$m_{3r} = f_2 / f \tag{20}$$

where f, f_1 and f_2 are linear functions of s_2 and c_2.
Noting the properties of rotation about $\hat{\mathbf{z}}_3$ the following may be deduced,

$$f_1^2 + f_2^2 = f^2 \left(\mathbf{pi}_{3o} \circ \mathbf{pi}_{3o} - l_{3r}^2\right) \tag{21}$$

This last equation is a polynomial of s_2, c_2, s_2^2, c_2^2 and $s_2 c_2$; and can be re-expressed in the following form,

$$\sum_{k=0}^{4} b_{4-k} t^{4-k} = 0 \tag{22}$$

where the coefficients are calculated symbolically from the model presented above. The parameters which constitute these coefficients reflect the kinematic relations between the successive arm axes and they can be calculated and stored for run-time use once the arm is calibrated. These parameters are all constant for a given arm except $\mathbf{pf}_{1r} \circ \mathbf{pf}_{1r}$ and l_{1o} which depend on the desired final location of the end-effector as described above. The fact that only two parameters need to be calculated highlights the computational efficiency of the described approach.

In (22), t is the tangent of half θ_2 and it is used to replace c_2 and s_2 as follows,

$$\left.\begin{aligned} c_2 &= \frac{1-t^2}{1+t^2} \\ s_2 &= \frac{2t}{1+t^2} \end{aligned}\right\} \tag{23}$$

Equation (22), which is a fourth degree polynomial, can be solved using a systematic non-iterative technique (Tranter, 1980). The resulting roots can successively be plugged back in equations (23) to work out the corresponding values of c_2 and s_2. These values are then employed to obtain the joint-displacement θ_2 using the atan2 function referred to above. The values of the local coordinates, n_{3r} and m_{3r}, may be calculated by using equations (19) and (20).

A numerically stable method to obtain m_{1o} and n_{1o} is to use equation (17) for n_{1o} and then obtain m_{1o} from the following equation,

$$m_{1o} = \left(\mathbf{p}_{2o}^{r} - d_2\hat{\mathbf{z}}_2\right) \circ \hat{\mathbf{y}}_1 \tag{24}$$

Finally, n_{3r}, m_{3r}, n_{3o}, m_{3o} are employed in equation (6) to obtain the corresponding values of θ_3. Similarly, n_{1r}, m_{1r}, n_{1o}, m_{1o} are used to obtain the corresponding values of θ_1.

As revealed by the polynomial in (22), the maximum number of arm configurations, N_{arm}, which correspond to a given end-effector position is four. In some cases, however, the geometrical relationships between the consecutive axes as well as the required position of p_f allow for the inverse position problem to be solved through the use of quadratic, rather quartic or higher, polynomials. Arms which exhibit this sort of simplification are said to have simple structures. Some of these cases are outlined in the next section.

5. Kinematic Synthesis of the Arm Mechanism

Most industrial robots are designed to have their successive axes either parallel or perpendicular to make a simplified closed form inverse position solution achievable. Researchers have repeatedly assigned the term, *simple structure*, to these robotic arms. The word "*simple*" usually implies that a non-iterative solution can be obtained for the inverse position problem of this particular structure. However, as the discussion in the previous section reveals, a non-iterative solution can still be obtained even for arms with arbitrarily positioned and directed joint-axes. A definition has been proposed for this term in the light of the conics theory (Smith and Lipkin, 1990). In the present section, a consistent simplified geometrical definition is introduced.

To gain understanding of the results obtainable from the fourth-degree polynomial equation (22), equations (13) and (14) along with the following two equations may be considered,

$$n_{3r}^2 + m_{3r}^2 = \mathbf{pi}_{3o} \circ \mathbf{pi}_{3o} - l_{3r}^2 \tag{25}$$

$$n_{1o}^2 + m_{1o}^2 = \mathbf{pf}_{1r} \circ \mathbf{pf}_{1r} - l_{1o}^2 \tag{26}$$

The four equations, (13), (14), (25) and (26), together are useful in studying the kinematic behaviour of the arm mechanism.

Essentially, the inverse position problem of the arm structure may be depicted as shown in Figure (3). In the figure, points p_f and p_i assume their local circular paths about the rotary axes, $\hat{\mathbf{z}}_1$ and $\hat{\mathbf{z}}_3$, creating two spatial circles Cz_1 and Cz_3, respectively, in two planes perpendicular to $\hat{\mathbf{z}}_1$ and $\hat{\mathbf{z}}_3$ with their centres located on the axes. Thus, a solution exists if a circle, Cz_2, that intersects both Cz_1 and Cz_3 simultaneously, can be drawn in a plane normal to $\hat{\mathbf{z}}_2$ with its centre located along it. As the analysis given in the previous section suggests, if the three axes are located and directed arbitrarily in space, a maximum of four different circles can be drawn about $\hat{\mathbf{z}}_2$ to satisfy this condition. Each circle intersects each of Cz_1 and Cz_3 at **one** point and hence, the four possible solutions.

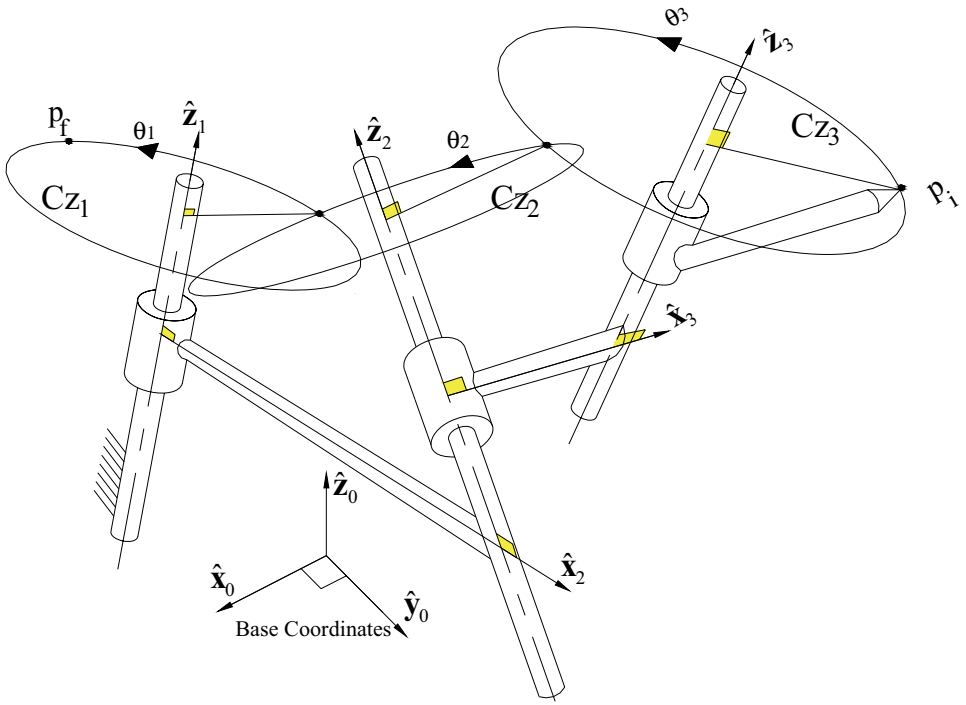

Figure 3. The Kinematic Behaviour of the Arm Joints.

As established in Appendix B, any two spatial circles may intersect at two points if, and only if, their corresponding axes lie in one and the same plane (this is the plane which perpendicularly halves the line connecting the two points of intersection). Therefore, in arms with ideal (non-calibrated) structures where $\hat{\mathbf{z}}_2$ lies in the same plane with either $\hat{\mathbf{z}}_1$ or $\hat{\mathbf{z}}_3$, the number of middle circles, Cz2, becomes **two**. In such a case, the complex mathematical aspects associated with the inverse position problem of the arm disappear and the solution can easily be obtained by using equations (13), (14), (25) and (26). For example, if $\hat{\mathbf{z}}_1$ and $\hat{\mathbf{z}}_2$ lie in one plane where $a_2 = 0$, the following procedure may be adopted for the solution;

- i. use equations (13) and (14) to express n_{3r} and m_{3r} as functions of m_{1o}.
- ii. use these functions in equation (25) to obtain the two roots of m_{1o}: $m_{1o}\big|_1$ and $m_{1o}\big|_2$,
- iii. use equation (26) to obtain the four corresponding values of n_{1o}: $n_{1o}\big|_1$, $-n_{1o}\big|_1$, $n_{1o}\big|_2$ and $-n_{1o}\big|_2$,

- iv. use equations (13) to obtain the two corresponding values of m_{3r}: $m_{3r}|_1$ and $m_{3r}|_2$; then use (14) to obtain the corresponding values of n_{3r}:. $n_{3r}|_1$ and $n_{3r}|_2$,
- v. combine the roots in the following order to obtain the required solutions,
- ($n_{1o}|_1$, $m_{1o}|_1$, $n_{3r}|_1$, $m_{3r}|_1$), ($-n_{1o}|_1$, $m_{1o}|_1$, $n_{3r}|_1$, $m_{3r}|_1$), ($n_{1o}|_2$, $m_{1o}|_2$, $n_{3r}|_2$, $m_{3r}|_2$) and ($-n_{1o}|_2$, $m_{1o}|_2$, $n_{3r}|_2$, $m_{3r}|_2$).

The corresponding four values of θ_2 may be obtained by solving equations (17) and (18) simultaneously for $\cos\theta_2$ and $\sin\theta_2$. Also, θ_1 and θ_3 are obtained by using equation (5).
The above mathematical procedure can be performed symbolically such that, closed form expressions are obtained for the three joint-displacements.
Similar simplified mathematical procedure may be used in cases with $\hat{\mathbf{z}}_1$ parallel to $\hat{\mathbf{z}}_2$. It may be noted that in designs where $\hat{\mathbf{z}}_2$ lies in one plane with $\hat{\mathbf{z}}_1$ and in another plane with $\hat{\mathbf{z}}_3$, the number of middle circles, Cz2, becomes **one** and the solution can be simplified even further. In such a case, the middle circle, Cz2, intersects both Cz1 and Cz3 at two points to produce the four possible solutions. An example may be sought in PUMA-type robots, whose nominal structures possess the following kinematic features,

$$a_2 = 0, \qquad \hat{\mathbf{y}}_1 \circ \hat{\mathbf{z}}_2 = -1 \qquad \text{and} \qquad \hat{\mathbf{y}}_3 \circ \hat{\mathbf{z}}_2 = 0$$

This makes it possible to obtain the solution for a non-calibrated PUMA arm substructure using the following procedure,

- i. obtain m_{1o} from equation (13)
- ii. obtain n_{3r} from equation (14)
- iii. obtain $\pm m_{3r}$ from equation (25)
- iv. obtain $\pm n_{1o}$ from equation (26)

Thus, the four possible configurations of the arm are given by the following root combinations,

(n_{1o}, m_{1o}, n_{3r}, m_{3r}), (n_{1o}, m_{1o}, n_{3r}, $-m_{3r}$), ($-n_{1o}$, m_{1o}, n_{3r}, m_{3r}) and ($-n_{1o}$, m_{1o}, n_{3r}, $-m_{3r}$).

Based on the above discussion it can be concluded that the middle axes $\hat{\mathbf{z}}_2$ must lie in one plane with either $\hat{\mathbf{z}}_1$ or $\hat{\mathbf{z}}_3$ for a simplified mathematical procedure to be realisable. Once this condition is satisfied, the four equations, (13), (14), (25) and (26) can be readily employed to obtain the inverse solution and therefore the arm structure can be described as *simple*.
In the next section, the procedure which is presented for the inverse position analysis of the wrist substructure is explained.

6. Inverse Kinematics of the Wrist

In the current context, the main task of the first two wrist joints (namely the fourth and fifth joints on the manipulator structure) is to displace the axis of the last joint (i.e. the sixth joint) from a given known orientation to a new desired direction in space.
Figure (4) depicts an arrangement of two revolute joints with their axes $\hat{\mathbf{z}}_4$ and $\hat{\mathbf{z}}_5$ pointing in the directions calculated using any suitable direct kinematic procedure featuring three consecutive rotations, $\theta_3\hat{\mathbf{z}}_3$, $\theta_2\hat{\mathbf{z}}_2$ and $\theta_1\hat{\mathbf{z}}_1$. At this specific pose, the axis of the sixth joint, $\hat{\mathbf{z}}_6^{\mathrm{i}}\big|_{5o}$, is also calculated using the same consecutive rotations, and it is now required to be orientated in the direction of $\hat{\mathbf{z}}_6^{\mathrm{f}}$. In the figure, the common normal $\hat{\mathbf{x}}_5$ is directed from $\hat{\mathbf{z}}_4$ to $\hat{\mathbf{z}}_5$ (where $\hat{\mathbf{x}}_5 = \hat{\mathbf{z}}_4 \times \hat{\mathbf{z}}_5$). At zero position $\hat{\mathbf{x}}_4$ is selected to coincide with $\hat{\mathbf{x}}_5$ such that two Cartesian coordinate systems $\hat{\mathbf{x}}_4\hat{\mathbf{y}}_4\hat{\mathbf{z}}_4$ and $\hat{\mathbf{x}}_5\hat{\mathbf{y}}_5\hat{\mathbf{z}}_5$ can be established. According to the concepts in (4) and (5), $\hat{\mathbf{z}}_6^{\mathrm{f}}$ can be described with respect to the $\hat{\mathbf{x}}_4\hat{\mathbf{y}}_4\hat{\mathbf{z}}_4$-frame in terms of local coordinates (n_{4r}, m_{4r} and l_{4r}). Also, $\hat{\mathbf{z}}_6^{\mathrm{i}}\big|_{5o}$ can be described with respect to the $\hat{\mathbf{x}}_5\hat{\mathbf{y}}_5\hat{\mathbf{z}}_5$-frame in terms of known local coordinates (n_{5o}, m_{5o} and l_{5o}).

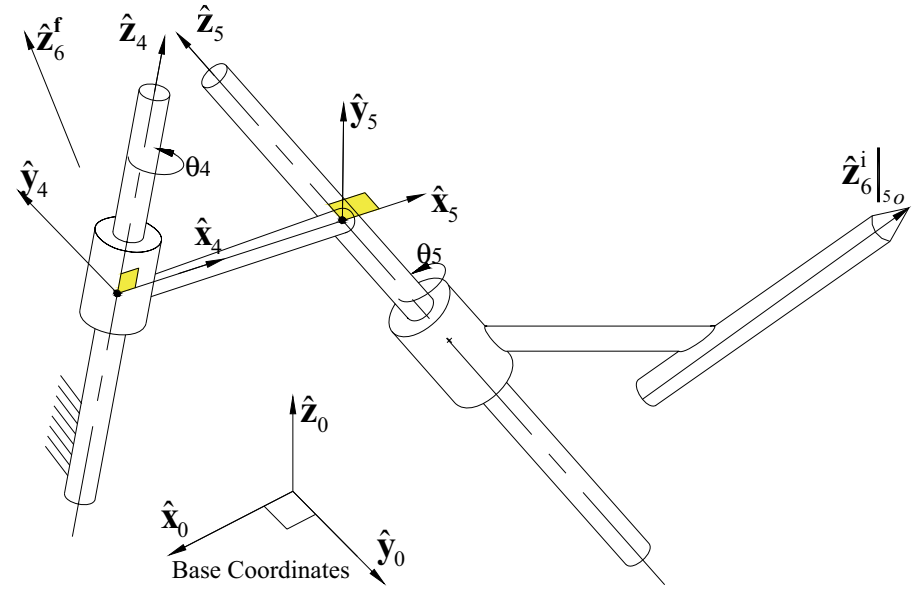

Figure 4. A 2R Arrangement Used for Orienting Vectors in Space.

It is understood that the vector $\hat{\mathbf{z}}_6^{\mathrm{f}}$ resulted from rotating another vector $\hat{\mathbf{z}}_6^{\mathrm{f}}\big|_{4o}$ about the $\hat{\mathbf{z}}_4$ axis by an angle, θ_4 (i.e. a $\theta_4\hat{\mathbf{z}}_4$-type rotation). The original vector, $\hat{\mathbf{z}}_6^{\mathrm{f}}\big|_{4o}$, can be expressed with respect to the $\hat{\mathbf{x}}_4\hat{\mathbf{y}}_4\hat{\mathbf{z}}_4$-frame in terms of local coordinates (n_{4o}, m_{4o} and l_{4o}), where n_{4o} and m_{4o} are unknowns to be worked out and l_{4o} is numerically obtained from $l_{4o} = l_{4r} = \hat{\mathbf{z}}_6^{\mathrm{f}} \circ \hat{\mathbf{z}}_4$.
The vector $\hat{\mathbf{z}}_6^{\mathrm{i}}\big|_{5r}$ which results from rotating $\hat{\mathbf{z}}_6^{\mathrm{i}}\big|_{5o}$ by an angle $\theta_5\hat{\mathbf{z}}_5$ may be expressed in the following form,

$$\hat{\mathbf{z}}_6^{\mathrm{i}}\big|_{5r} = (n_{5o}c_5 - m_{5o}s_5)\hat{\mathbf{x}}_5 + (n_{5o}s_5 + m_{5o}c_5)\hat{\mathbf{y}}_5 + l_{5o}\hat{\mathbf{z}}_5 \tag{27}$$

where c_5 and s_5 stand for $\cos\theta_5$ and $\sin\theta_5$ respectively.
A property of rotation about $\hat{\mathbf{z}}_4$ may be stated as,

$$l_{4o} = (n_{5o}s_5 + m_{5o}c_5)\hat{\mathbf{y}}_5 \circ \hat{\mathbf{z}}_4 + l_{5o}\hat{\mathbf{z}}_5 \circ \hat{\mathbf{z}}_4 \tag{28}$$

This last expression (28) is a linear equation in s_5 and c_5. This equation may be re-expressed in a polynomial form as follows,

$$\sum_{k=0}^{2} b_{2-k}t^{2-k} = 0 \tag{29}$$

where t is the tangent of half θ_5 and b_j is the coefficient of the jth power term.
It could be concluded from equation (29), which is a second degree polynomial, that the number of the wrist configurations, N_{wrist}, which correspond to the required orientation of $\hat{\mathbf{z}}_6^f$ is ≤ 2.
Once θ_5 is obtained, m_{4o} and n_{4o} can be worked out as follows;

$$\left.\begin{aligned} n_{4o} &= n_{5o}c_5 - m_{5o}s_5 \\ m_{4o} &= \left(n_{5o}s_5 + m_{5o}c_5\right)\hat{\mathbf{y}}_5 \circ \hat{\mathbf{y}}_4 + l_{5o}\hat{\mathbf{z}}_5 \circ \hat{\mathbf{y}}_4 \end{aligned}\right\} \tag{30}$$

Finally, n_{4r}, m_{4r}, n_{4o} and m_{4o} are employed in equation (6) to obtain the corresponding values of θ_4.
From the analysis presented in this and the previous sections, it can be concluded that the maximum number of configurations of a spherical-wrist manipulator structure which correspond to any given position and orientation at the end-effector is eight. The actual number of configurations, N, is calculated by,

$$N = N_{arm}N_{wrist} \tag{31}$$

In spherical-wrist manipulators, each arm configuration corresponds to two possible wrist configurations as indicated by equation (31).

7. Completing the Full Pose

Once the first five joints on the manipulator structure have performed consecutive rotations ($\theta_i\hat{\mathbf{z}}_i$, where $i = 1,2,...5$) to place the sixth joint axis at its desired position and orientation, one final rotation ($\theta_6\hat{\mathbf{z}}_6$), will be performed to align any side axis on the end-effector with its desired direction. The term "side axis" here refers to any axis, on the end-effector Cartesian frame, whose direction is influenced by rotations performed about $\hat{\mathbf{z}}_6$. This final part of the inverse kinematic procedure is a straight forward application of the model presented in equations (3) to (6) to calculate the angle of rotation. However, it worth noting here that this final step of the analysis is preceded by a direct kinematic procedure to calculate the updated direction of the side axis after five consecutive rotations, $\theta_5\hat{\mathbf{z}}_5, \theta_4\hat{\mathbf{z}}_4, \theta_3\hat{\mathbf{z}}_3, \theta_2\hat{\mathbf{z}}_2$ and $\theta_1\hat{\mathbf{z}}_1$, have been performed.

8. The Inverse Solution Procedure

Figure (5) depicts a flow chart that has been designed to explain the procedure proposed here for the inverse position analysis of manipulators. For spherical-wrist manipulators, the procedure produces eight sets of solutions in a non-iterative fashion. However, for calibrated robotic structures, the eight solutions are obtained in a simple iterative approach which does not involve any Jacobian matrix computations. By virtue of the concepts presented, the various solutions may be calculated simultaneously if parallel computing facilities are available.

In the present approach, the arm is assigned the task of positioning any point on the sixth joint-axis at its required spatial location. The closest point on the sixth-joint axis to the fifth joint-axis may be conveniently selected for this purpose. This point will be referred to in the following discussion as p_0^i. The four joint-displacement solutions which correspond to this positioning task are therefore obtained using the models presented above and saved in four three-element vectors, $\mathbf{v}_j$, where j=1,2,3 and 4.

At arm configuration number j, the wrist joints align the sixth joint-axis with its required final orientation, as previously described, and the two corresponding solutions are accordingly obtained and saved in a pair of two-elements vectors, $\mathbf{w}_{jk}$, where k may assume the values of 1 or 2. To this end, a set of eight joint-displacement solutions have been obtained. If the robot was of the spherical-wrist type these solutions should accurately represent the required joint-displacements and no iterations would be required.

Calibrated robots, however, are not likely to have their last three joint-axes intersecting at a common point (i.e. the spherical-wrist property is lost), the motions performed by the wrist joints will displace the point which was previously positioned by the arm to eight new locations, p_0^{jk}, corresponding to the wrist solutions obtained.

At location number jk, the instantaneous position vector, $\mathbf{p}_0^{jk}$, of the displaced point may be calculated, using a suitable direct kinematic procedure, and compared to the required position vector $\mathbf{p}_0^n$ where the net radial error, e_{jk}, is calculated as follows,

$$e_{jk} = \left\| \mathbf{p}_0^n - \mathbf{p}_0^{jk} \right\| \tag{32}$$

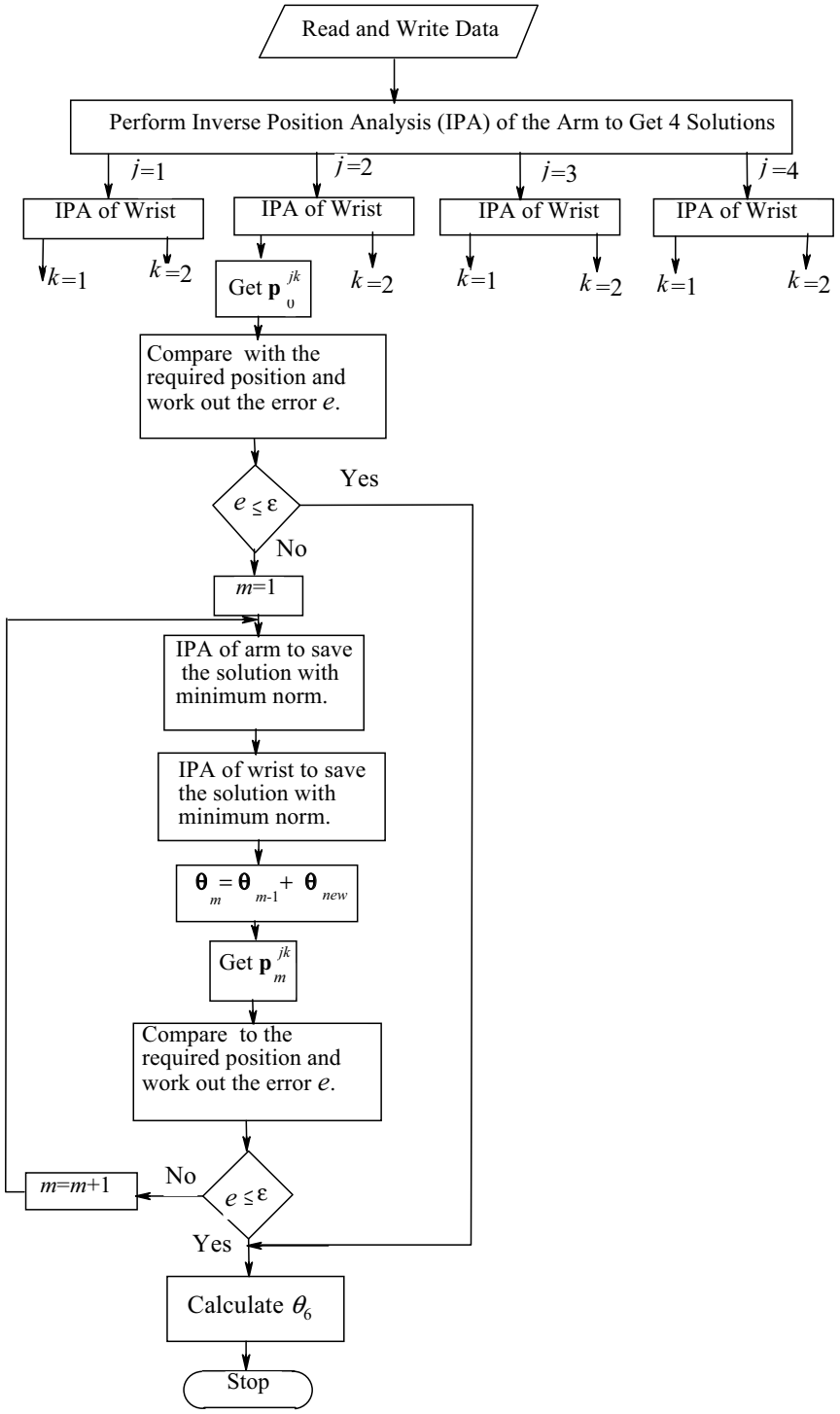

Figure 5. Inverse Position Analysis of Robots Using Elementary Motions.

If the calculated value for e_{jk} does not fall within an allowable error zone, the calculations proceed such that at iteration number m, the arm sets out from the most updated configuration number $jk(m\text{-}1)$ to position point p_{m-1}^{jk} in the required location, $\mathbf{p}_0^n$. The four solutions obtained may be stored in four three-

element vectors whose norms are subsequently calculated and compared. Only the vector which corresponds to minimum norm, $\mathbf{v}_{jk}^{m}$, may be saved in the memory and the other solutions would be discarded. This vector is referred to here as the **arm elementary-motions vector** because it contains fractional quantities of elementary joint-displacements.
The two corresponding wrist solutions may then be obtained and stored in a pair of two-element vectors whose norms will also be calculated and compared. The vector with minimum norm, $\mathbf{w}_{jk}^{m}$, is subsequently saved while the other vector may be disposed of. In the current context, $\mathbf{w}_{jk}^{m}$ is designated as the **wrist elementary-motions vector** because it contains small values of joint-displacements.
The new displaced location of the positioned point may then be calculated and compared with the required location as per equation (32). When the radial error is small enough, the final joint-displacement vector, $\mathbf{v}_{jk}^{n}$, of the arm group which corresponds to solution number *jk* may be calculated as follows,

$$\mathbf{v}_{jk}^{n} = \mathbf{v}_{j} + \sum_{m=1}^{M} \mathbf{v}_{jk}^{m} \tag{33}$$

where *M* is the corresponding number of iterations.

The vector, $\mathbf{w}_{jk}^{n}$, which corresponds to the *jk*-solution of the wrist is calculated as;

$$\mathbf{w}_{jk}^{n} = \mathbf{w}_{jk} + \sum_{m=1}^{M} \mathbf{w}_{jk}^{m} \tag{34}$$

Once the *jk*-solution for the first five joint-displacements has been obtained, the corresponding displacement of the last joint may simply be calculated.
The iterative technique presented here utilises the physical kinematic behaviour of manipulator joints and therefore fast and singularity-proof convergence may be assured. The technique does not require initial guesses introduced into the model.
In the next section a numerical example is given where the inverse position solutions will be produced for a PUMA-type robot of both calibrated and ideal structures.

9. Numerical Example

A PUMA-like manipulator with six revolute joints is selected for the example. The dimensions of the spherical-wrist structure of the manipulator are given in Table (1). The dimensions of the non-spherical-wrist version of the same manipulator are similar to those given in Table (1) except for the locations of the fourth and fifth joint-axes which were displaced to (-128.0, 818.51 and 205.04 mm) and (-130.5, 802.0 and 180.4 mm) respectively.

	Direction Cosines of Joint-axes			Axes Locations (mm)		
Axes	z_x	z_y	z_z	p_x	p_y	p_z
z_1	-0.0871557	0.02255767	0.9848077	-1.0	-9.0	8.0
z_2	-0.9961946	0.0001274	-0.0871557	5.0	-5.0	198.0
z_3	-0.9961947	0.05233595	0.0696266	-68.0	438.0	195.0
z_4	0.02233595	-0.9993908	0.02681566	-130.5	808.5	177.0
z_5	0.99975050	-0.0223359	0.00009744	-130.5	808.5	177.0
z_6	0.02489949	0.9996253	0.00012081	-130.0	808.5	177.0

Table 1. Cartesian Dimensions of a Spherical-wrist Manipulator.

In both cases, the initial and final locations of the Tool Centre Point (TCP) of the end-effector are given with respect to the base coordinates as, -120.54, 1208.36 and 175.095 and, –400.0, –400.0 and 1009.0 mm respectively. The initial and final orientations of the end-effector are given in terms of an Euler ZYZ-system as: 88.5733, 89.9604 and 89.722 and, 120.0, –20.0 and 150.0 degrees respectively.

The models proposed in this paper were used to calculate the inverse position solutions for both the spherical-wrist and general manipulator structures and the results are displayed in Tables (2) and (3) respectively. The angular displacements given in these tables are in degrees.

	θ_1	θ_2	θ_3	θ_4	θ_5	θ_6
Sol. No. 1	-34.45	-163.09	64.67	86.12	-36.06	-130.97
Sol. No. 2	-34.45	-163.09	64.67	-85.75	31.73	58.63
Sol. No. 3	-47.14	-104.39	-72.4	19.01	-84.81	154.74
Sol. No. 4	-47.14	-104.39	-72.4	-160.03	80.47	-20.04
Sol. No. 5	104.39	-72.90	64.57	24.26	85.22	2.38
Sol. No. 6	104.39	-72.90	64.57	-156.27	-89.56	177.24
Sol. No. 7	117.07	-11.05	-72.30	68.50	28.82	68.23
Sol. No. 8	117.07	-11.05	-72.30	-120.58	-33.16	-122.18

Table 2. Inverse Position Solutions for the Spherical-wrist Robot.

	θ_1	θ_2	θ_3	θ_4	θ_5	θ_6
Sol. No. 1	-39.20	-162.93	66.79	86.5	-36.82	-125.19
Sol. No. 2	-30.78	-162.92	70.95	-73.54	32.47	68.51
Sol. No. 3	-48.12	-106.90	-68.18	19.18	-83.65	156.37
Sol. No. 4	-46.46	-103.38	-65.35	-158.64	72.85	-17.25
Sol. No. 5	105.11	-73.14	67.49	24.37	87.28	0.42
Sol. No. 6	103.60	-70.98	72.08	-154.89	-98.19	173.67
Sol. No. 7	120.24	-11.00	-68.57	65.31	29.99	60.59
Sol. No. 8	114.00	-11.34	-62.96	-133.30	-37.94	-134.91

Table 3. Inverse Position Solutions for the Non-spherical-wrist Robot.

The solutions obtained for the spherical-wrist manipulator did not involve iterations at all. However, a maximum of 4 iterations were used for the non-spherical-wrist manipulator. In most cases the number of iterations was 2 except for the second and first solutions were this number was 3 and 4 respectively. This demonstrates the numerical efficiency of the proposed models.

10. Conclusions

The work presented in this paper introduces a technique for inverse position analysis of revolute-joint manipulators. The analysis developed results in simplified solutions for both the arm and the wrist subassemblies. These solutions are obtained in form of polynomials whose coefficients can be simply calculated for a given manipulator structure. The technique can be used to obtain inverse kinematic solutions for both spherical-wrist and calibrated manipulator structures.

The technique results in obtaining multiple sets of the joint-motor displacements which correspond to a given pose at the end-effector. This enables the trajectory designer to the select the joint-trajectory which best fits a desired manipulator task.

Appendix A

To relate a pair of successive axes on a manipulator structure, the direction cosines of the two axes are given (with respect to a Cartesian base frame), together with a position vector describing a point on each axis. These spatial particulars are defined in Figure (A) as $\hat{\mathbf{z}}_i$ and $\mathbf{p}_{0i}$ for the joint axis number i, and $\hat{\mathbf{z}}_{i+1}$ and $\mathbf{p}_{0(i+1)}$ for joint-axis number i+1. The procedure kicks off by calculating the common normal, $\mathbf{x}_{i+1}$ as follows;

$$\mathbf{x}_{i+1} = \hat{\mathbf{z}}_i \times \hat{\mathbf{z}}_{i+1} \tag{A.1}$$

where the following condition is employed;

$$\textit{if } \left\| \hat{\mathbf{z}}_i \times \hat{\mathbf{z}}_{i+1} \right\| = 0 \quad \textit{then } \mathbf{x}_{i+1} = \left(\mathbf{p}_{0(i+1)} - \mathbf{p}_{0i} \right) - \hat{\mathbf{z}}_i \left[\left(\mathbf{p}_{0(i+1)} - \mathbf{p}_{0i} \right) \circ \hat{\mathbf{z}}_i \right] \tag{A.2}$$

The unit vector, $\hat{\mathbf{x}}_{i+1}$, is then calculated as follows;

$$\hat{\mathbf{x}}_{i+1} = \frac{\mathbf{x}_{i+1}}{\left\| \mathbf{x}_{i+1} \right\|} \tag{A.3}$$

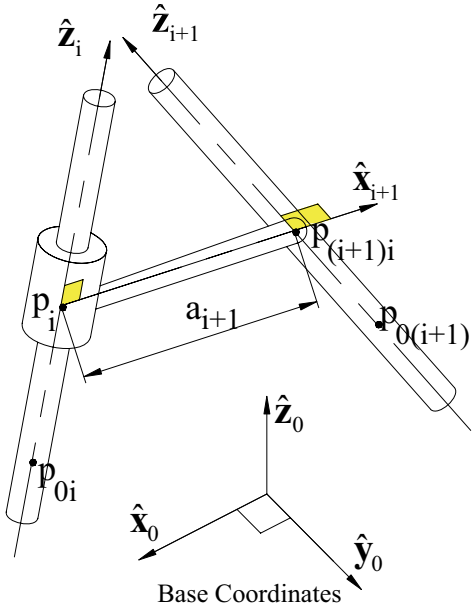

Figure A. Relating Successive Axes with a Common Normal.

The shortest distance, a_{i+1}, separating the two axes is calculated as follows;

$$a_{i+1} = \left(\mathbf{p}_{0(i+1)} - \mathbf{p}_{0i} \right) \circ \hat{\mathbf{x}}_{i+1} \tag{A.4}$$

The intersection of $\hat{\mathbf{x}}_{i+1}$ with $\hat{\mathbf{z}}_i$ is defined by a position vector $\mathbf{p}_i$, which is obtained from;

$$\mathbf{p}_i = \mathbf{p}_{0i} + b_i \hat{\mathbf{z}}_i \tag{A.5}$$

where

$$b_i = \frac{\left(\hat{\mathbf{z}}_{i+1} \times \hat{\mathbf{x}}_{i+1}\right) \circ \left(\mathbf{p}_{0(i+1)} - \mathbf{p}_{0i}\right)}{\left(\hat{\mathbf{z}}_{i+1} \times \hat{\mathbf{x}}_{i+1}\right) \circ \hat{\mathbf{z}}_i} \tag{A.6}$$

which is subject to the condition, $if \quad \left(\hat{\mathbf{z}}_{i+1} \times \hat{\mathbf{x}}_{i+1}\right) \circ \hat{\mathbf{z}}_i = 0 \quad then \quad b_i = 0$ (A.7)

The intersection of $\hat{\mathbf{x}}_{i+1}$ with $\hat{\mathbf{z}}_{i+1}$ is defined by a position vector $\mathbf{p}_{i(i+1)}$, which is calculated from;

$$\mathbf{p}_{i(i+1)} = \mathbf{p}_i + a_{i+1} \hat{\mathbf{x}}_{i+1} \tag{A.8}$$

Appendix B

Claim:
Any two spatial circles intersect at two points if, and only if, their axes lie in one and the same plane.

Proof:
Figure (B) depicts two spatial circles, C_1 and C_2, and their axes, $\hat{\mathbf{z}}_1$ and $\hat{\mathbf{z}}_2$ respectively. The circles intersect one another at two points, s_1 and s_2. To prove that $\hat{\mathbf{z}}_1$ and $\hat{\mathbf{z}}_2$ must lie in one and the same plane, the centres of the two circles, Pc_1 and Pc_2, are connected to the point, s_3, which divides the line $\overline{s_1 s_2}$ into two equal parts.

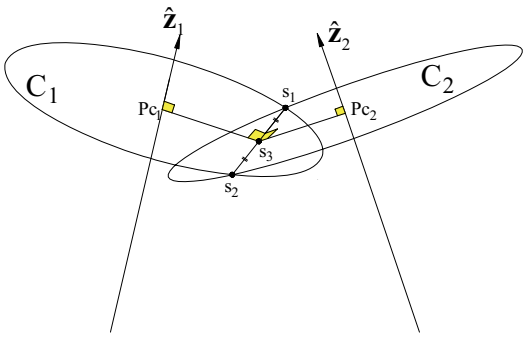

Figure B. Two-point Intersection of Spatial Circles.

- $\overline{s_1 s_2}$ lies in a plane perpendicular to $\hat{\mathbf{z}}_1$ and therefore $\overline{s_1 s_2}$ is perpendicular to $\hat{\mathbf{z}}_1$.
- From planar geometry, $\overline{s_1 s_2}$ is perpendicular to the line $\overline{\mathrm{Pc}_1 s_3}$.
- Therefore $\overline{s_1 s_2}$ is perpendicular to the plane which contains the two intersecting lines, $\hat{\mathbf{z}}_1$ and $\overline{\mathrm{Pc}_1 s_3}$. Let this plane be referred to as PN1.
- Similarly, it could be established that $\overline{s_1 s_2}$ is also perpendicular to the plane which contains the two intersecting lines, z_2 and $\overline{\mathrm{Pc}_2 s_3}$. This plane may be referred to as PN2.
- A general conclusion may now be drawn that, PN1 is parallel to PN2.
- However, PN1 and PN2 share one common point, s_3.
- Therefore, the two planes coincide and $\hat{\mathbf{z}}_1$, $\overline{\mathrm{Pc}_1 s_3}$, $\hat{\mathbf{z}}_2$ and $\overline{\mathrm{Pc}_2 s_3}$ must all lie in one and the same plane.

11. References

Chiaverini, S., Siciliano, B. and Egeland, O. (1994), Review of the Damped Least-Squares Inverse kinematics with Experiments on an Industrial Robot Manipulator, IEEE Trans. Control Syst. Technol., Vol. 2, No. 2, pp. 123-134.

Coelho, P. H. G. and Nunes, L. F. A. (1986), Application of Kalman Filtering to Robot Manipulators, In: *Recent Trends in Robotics: Modelling, Control and Education*. Jamshidi, M., Luh, L. Y. S. and Shahinpoor, M. (Ed.), pp. 35-40, Elsevier Science Publishing Co., Inc.

Denavit, J. and Hartenberg, R. S. (1955), A Kinematic Notation for Low Pair Mechanisms Based on Matrices, *J. Appl. Mech.-Trans. ASME*, Vol. 22, June 1955, pp. 215-221.

Duffy, J. and Crane C. (1980), A Displacement Analysis of the General Spatial 7-Link, 7R Mechanism, *Mech. Mach. Theory*, Vol. 15, No. 3-A, pp. 153-169.

Goldenberg, A. A., Benhabib, B. and Fenton, R. G. (1985), A Complete Generalised Solution to the Inverse Kinematics of Robots, *IEEE. Trans. Robot Autom*, Vol. RA-1, No. 1, pp. 14-20.

Gu, Y.-L. and Luh, J. Y. S. (1987), Dual-Number Transformation and Its Application to Robotics, *IEEE. Trans. Robot Autom*, Vol. RA-3, No. 6, pp. 615-623.

Gupta, K. (1984), A Note on Position Analysis of Manipulators, *Mech. Mach. Theory*, Vol. 19, No. 1, pp. 5-8.

Hayati, S. and Roston, G. (1986), Inverse Kinematic Solution for Near-Simple Robots and Its Application to Robot Calibration, In: *Recent Trends in Robotics: Modelling, Control and Education.*, Jamshidi, M., Luh, L. Y. S. and Shahinpoor, (Ed.), M. Elsevier Science Publishing Co., Inc, pp. 41-50.

Her, M.-G, Yen, C.-Y., Hung, Y.-C. and Karkoub, M. (2002), Approximating a Robot Inverse Kinematics Solution Using Fuzzy Logic Tuned by Genetic Algorithms, *Int. J. Adv. Manuf. Technol*, Vol. 20, pp. 372-380.

Kohli, D. and Osvatic, M. (1993), Inverse Kinematics of General 6R and 5R,P Spatial Manipulators, *ASME J. Mech. Des.*, Vol. 115, Dec. 1993, pp. 922-930.

Lee, H.-Y. and Liang, C. G. (1988a), A New Vector Theory for the Analysis of Spatial Mechanisms, *Mech. Mach. Theory*, Vol. 23, No. 13, pp. 209-217.

Lee, H.-Y. and Liang, C. G. (1988b), Displacement Analysis of the General Spatial 7-Link 7R Mechanism, *Mech. Mach. Theory*, Vol. 23, No. 13, pp. 219-226.

Lee, H.-Y., Reinholtz, C. F. (1996), Inverse Kinematics of Serial-Chain Manipulators, *J. Mech. Des.-Trans. ASME*, Vol. 118, Sept. 1996, pp. 396-404.

Mahalingam, S. and Sharan (1987), A., The Nonlinear Displacement Analysis of Robotic Manipulators Using the Complex Optimisation Method, *Mech. Mach. Theory*, Vol. 22, No. 1, pp. 89-95.

Manocha, D. and Canny, J. F. (1992), Real Time Inverse Kinematics for General 6R Manipulators, *Proceedings of IEEE Conf. on Robotics and Automation*, pp. 383-389, Nice-France, May 1992.

Manseur, R. and Doty, K. (1992a), A Complete Kinematic Analysis of Four-Revolute-Axis Robot Manipulators, *Mech. Mach. Theory*, Vol. 27, No. 5, pp. 575-586.

Manseur, R. and Doty, K. (1992b), Fast Inverse Kinematics of Five-Revolute-Axis Robot Manipulators, *Mech. Mach. Theory*, Vol. 27, No. 5, pp. 587-597.

Manseur, R. and Doty, K. (1989), A Robot Manipulator with 16 Real Inverse Kinematic Solution Sets, *Int. J. Robot Res*, Vol. 8, No. 5, pp. 75-79.

Manseur, R. and Doty, K. (1988), Fast Algorithm for Inverse Kinematic Analysis of Robot Manipulators, *Int. J. Robot Res*, Vol. 7, No. 3, pp. 52-63.

Manseur, R. and Doty, K. (1996), Structural Kinematics of 6-Revolute-Axis Robot Manipulators, *Mech. Mach. Theory*, Vol. 31, No. 5, pp. 647-657.

Pieper, D. L. and Roth, B. (1969), The Kinematics of Manipulators Under Computer Control, *Proceedings of 2nd Int. Congress on the Theory of Machines and Mechanisms*, Vol. 2, Zakopane, Poland, pp. 159–168.

Poon, J. K. and Lawrence, P. D. (1988), Manipulator Inverse Kinematics Based on Joint Functions, *Proceedings of IEEE Conf. on Robotics and Automation*, Philadelphia, pp. 669-674.

Pradeep, A. K., Yoder, P. J. and Mukundan, R. (1989), On the Use of Dual-Matrix Exponentials in Robotic Kinematic, *Int. J. Robot Res*, Vol. 8, No. 54, pp. 57-66.

Raghavan, M. and Roth, B. (1989), Kinematic Analysis of the 6R Manipulator of General Geometry, *Proceedings of the 5th Int. Symposium on Robotics Research*, Tokyo, pp. 263-269.

Smith, D. R. and Lipkin, H. (1990), Analysis of Fourth Order Manipulator Kinematics Using Conic Sections, *Proceedings of IEEE Conf. on Robotics and Automation*, Cincinnati, pp. 274-278.

Sultan, I. A. (2000), On the Positioning of Revolute-Joint Manipulators, *J. of Robot Syst*, Vol. 17, No. 8, pp 429-438.

Sultan, I. A. and Wager, J. G. (1999), User-Controlled Kinematic Modelling, *Adv. Robot.*, Vol. 12, No. 6, pp 663-677.

Sultan, I. A. and Wager, J. G. (2001), A ϕ-Model Solution for the Inverse Position Problem of Calibrated Robots Using Virtual Elementary Motions, *Inverse Probl. Eng.*, Vol. 9, No. 3, pp. 261-285.

Sultan, I. A. (2002), A Numerical Solution for Determinantal Polynomials with Application to Robot Kinematics, *Proceedings of the 4th Int. Conf. on Modelling and Simulation*, Melbourne.

Tsai, L.-W. and Morgan, A. P. (1985), Solving the Kinematics of the Most General Six- and Five-Degree-of-Freedom Manipulators by Continuation Methods, *ASME J. Mech, Transm and Autom Des*, Vol. 107, June 1985, pp. 189-199.

Tranter, C. J. (1980), *Techniques of Mathematical Analysis*. UNIBOOKS, Hodder and Stoughton, London.

Wang, K. and Bjorke, O. (1989), An Efficient Inverse Kinematic Solution with a Closed Form for Five-Degree-of-Freedom Robot Manipulators with a Non-Spherical Wrist, *Annals of CIRP*, Vol. 38, pp. 365-368.

Wang., L. T. and Chen, C. C. (1991), A Combined Optimisation Method for Solving the Inverse Kinematics Problem of Mechanical Manipulators, *IEEE. Trans. Robot Autom*, Vol. 7, No. 4, pp. 489-499.

Yang, A. T. and Freudenstein, F. (1964), Application of Dual-Numbers Quaternion Algebra to the Analysis of Spatial Mechanisms, *J. Appl. Mech.-Trans. ASME*, June 1964, pp. 300-308.

Zhang, P.-Y., Lu, T.-S. and Song, L.- B. (2005), RBF networks-based inverse kinematics of 6R manipulator, *Int J Adv Manuf Technol*., Vol. 26, pp. 144–147